Accelerated Publications

Picomolar Transition State Analogue Inhibitors of Human 5′-Methylthioadenosine Phosphorylase and X-ray Structure with MT-Immucillin-A†

Vipender Singh,‡,§ Wuxian Shi,‡,§ Gary B. Evans,|| Peter C. Tyler,|| Richard H. Furneaux,|| Steven C. Almo,§ and Vern L. Schramm*,§

Department of Biochemistry, Albert Einstein College of Medicine, Bronx, New York 10461, and Carbohydrate Chemistry Team, Industrial Research Limited, P.O. Box 31310, Lower Hutt, New Zealand

Received October 13, 2003; Revised Manuscript Received November 13, 2003

ABSTRACT: Methythioadenosine phosphorylase (MTAP) functions solely in the polyamine pathway of mammals to remove the methylthioadenosine (MTA) product from both spermidine synthase (2.5.1.16) and spermine synthase (2.5.1.22). Inhibition of polyamine synthesis is a validated anticancer target. We designed and synthesized chemically stable analogues for the proposed transition state of human MTAP on the basis of the known ribooxacarbenium character at all reported *N*-ribosyltransferase transition states [Schramm, V. L. (2003) *Acc. Chem. Res. 36*, 588−596]. Methylthio-immucillin-A (MT-ImmA) is an iminoribitol tight-binding transition state analogue inhibitor with an equilibrium dissociation constant of 1.0 nM. The immucillins resemble the ribooxacarbenium ion transition states of *N*-ribosyltransferases and are tightly bound as the N4′ cations. An ion pair formed between the iminoribitol cation and phosphate anion mimics the ribooxacarbenium cation−phosphate anion pair formed at the transition state and is confirmed in the crystal structure. The X-ray crystal structure of human MTAP with bound MT-Imm-A also reveals that the 5′-methylthio group lies in a flexible hydrophobic pocket. Substitution of the 5′-methylthio group with a 5′-phenylthio group gives an equilibrium binding constant of 1.0 nM. Methylthio-DADMe-immucillin-A is a pyrrolidine analogue of the transition state with a methylene bridge between the 9-deazaadenine group and the pyrrolidine ribooxacarbenium mimic. It is a slow-onset inhibitor with a dissociation constant of 86 pM. Improved binding energy with DADMe-immucillin-A suggests that the transition state is more closely matched by increasing the distance between leaving group and ribooxacarbenium mimics, consistent with a more dissociative transition state. Increasing the hydrophobic volume near the 5′-position at the catalytic site with 5′-phenylthio-DADMe-immucillin-A gave a dissociation constant of 172 pM, slightly weaker than the 5′-methylthio group. *p*-Cl-phenylthio-DADMe-immucillin-A binds with a dissociation constant of 10 pM (K_m/K_i* value of 500000), the tightest binding inhibitor reported for MTAP. These slow-onset, tight-binding transition state analogue inhibitors are the most powerful reported for MTAP and have sufficient affinity to be useful in inhibiting the polyamine pathway.

Cellular polyamines and the expression of polyamine pathway enzymes increase on rapid cell division (*1*). Depletion of the polyamines has been shown to be growth inhibitory and in some cases to restore transformed cells to the normal phenotype (*2*). The proof of concept for targeting the polyamine pathway as an anticancer approach has come from studies on α-difluoromethylornithine (DFMO), a covalent inactivator of ornithine decarboxylase (ODC), the committed step of polyamine biosynthesis (reviewed in ref *3*). Inhibitors of polyamine synthesis have anticancer activity in animal models and have been proposed for cancer chemoprevention. Although inhibition of polyamine biosynthesis is a validated cancer chemotherapeutic approach, ornithine decarboxylase has proven a difficult target because of its rapid turnover in mammalian cells and associated toxicity of anti-ODC agents (*4*−*6*). We selected methythioadenosine phosphorylase (MTAP)[1] as a potential target for

† Supported by research grants from the National Institutes of Health and the New Zealand Foundation for Science and Technology.

* To whom correspondence should be addressed. E-mail: vern@aecom.yu.edu. Phone: (718) 430-2813. Fax: (718) 430-8565.

‡ Equal contributors to this work.

§ Albert Einstein College of Medicine.

|| Industrial Research Limited.

[1] Abbreviations: MTA, 5′-methylthioadenosine; MTAP, 5′-methylthioadenosine phosphorylase; PNP, purine nucleoside phosphorylase; MT-ImmA, MT-immucillin-A [(1*S*)-1-(9-deazaadenin-9-yl)-1,4-dideoxy-1,4-imino-5-methylthio-D-ribitol]; phenylthio-immucillin-A, (1*S*)-1-(9-deazaadenin-9-yl)-5-phenylthio-1,4-dideoxy-1,4-imino-D-ribitol; MT-DADMe-immucillin-A, (3*R*,4*S*)-1-[(9-deazaadenin-9-yl)methyl]-3-hydroxy-4-(methylthiomethyl)pyrrolidine; benzylthio-DADMe-immucillin-A, (3*R*,4*S*)-1-[(9-deazaadenin-9-yl)methyl]-3-hydroxy-4-(benzylthiomethyl)pyrrolidine; *p*-Cl-phenylthio-DADMe-immucillin-A, (3*R*,4*S*)-1-[(9-deazaadenin-9-yl)methyl]-3-hydroxy-4-(4-chlorophenylthiomethyl)pyrrolidine.

10.1021/bi0358420 CCC: $27.50
Published on Web 12/09/2003

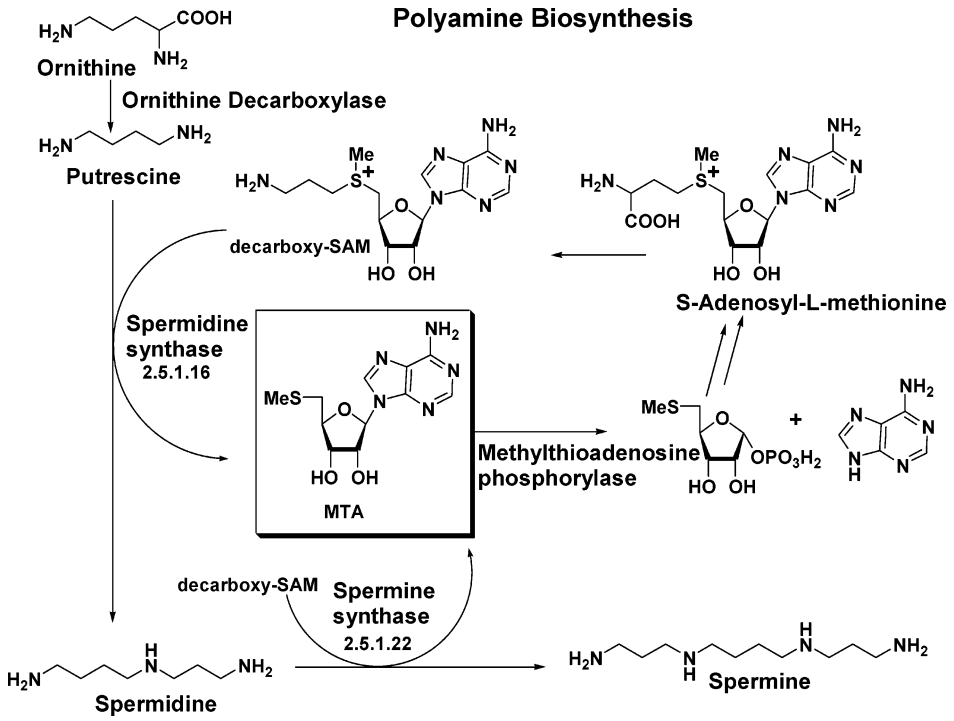

FIGURE 1: Pathway of polyamine biosynthesis. The committed step of the pathway forms putrescine from ornithine. In the two subsequent steps, transfer of two propylamine groups from decarboxy-SAM forms spermine and two methylthioadenosine molecules. MTAP is the only route for recycling the adenine to ATP and the methylthioribose to methionine.

transition state analogue design because of its exclusive function in the polyamine pathway and our success in design of inhibitors for the closely related reaction catalyzed by purine nucleoside phosphorylase (*7*−*9*). The goal is to provide powerful and specific inhibitors of MTAP. Such inhibitors may prove useful in resolving the conflicting and controversial questions of MTAP and polyamine levels in biological systems.

Methylthioadenosine (MTA) is a product of the reactions catalyzed by both spermidine and spermine synthases and thus has the potential to provide product feedback at two sequential sites in the synthetic pathway (Figure 1). The only means of metabolizing MTA in mammals is phosphorolysis by MTAP. Efficient inhibition of MTAP may cause a buildup in MTA concentration and a feedback inhibition of polyamine synthases. However, in yeast cultures, genetic deletion of the MTAP gene increased ODC activity 8-fold and increased total polyamine levels. It is proposed that 4-methylthio-2-oxobutanoic acid, a downstream product of MTAP activity, regulates ODC expression and polyamine formation in both yeast and cultured human MCF-7 breast cancer adenocarcinoma cell lines (*10*). In these cases, it is proposed that MTAP deletion may increase polyamines. However, in cell cultures, accumulation of MTA differs from that in mammalian tissues, and the effects of reversible whole-animal MTAP inhibition have yet to be resolved. Independent of the downstream effects, the presence of MTA has been reported to be antiapoptotic in cultured normal rat hepatocytes but proapoptotic in human hepatoma cells (*11*). Studies on the physiologic effects of MTAP would be possible if powerful and specific inhibitors were available.

A common gene deletion in human adult T-cell leukemia includes the MTAP locus. One role of MTAP is to regenerate adenine from MTA. MTAP deficiency prevents adenine recycling via adenine phosphoribosyltransferases and places extra demands on the de novo purine pathway of these cells. On the basis of this difference from normal cells, MTAP-deficient cells have increased susceptibility to interruption of purine synthesis, and it has been proposed to treat such cancers with antimetabolites of the de novo pathway (*12*). If suitable MTAP inhibitors were available, MTAP deficiency could be imposed on all rapidly dividing cells and might cause increased selectivity to purine antimetabolite therapy.

EXPERIMENTAL PROCEDURES

Materials. MTA, buffers, and other biochemical reagents were purchased from Sigma. The cDNA for human MTAP was generously provided by Drs. Carson and Rosenbech of Scripps Institute, La Jolla, CA (*13*). The expression vector and Ni-NTA chromatography medium were products of Qiagen. Centricon and Microcon filters were purchased from Amicon Inc. A Pharmacia Biotech FPLC was used for protein purification.

Human MTAP. Human MTAP was overexpressed in *Escherichia coli* BL21(DE3) using the pQE32 expression vector. A 1 L culture of *E. coli* transformed with a human MTAP clone was induced with 0.5 mM isopropyl β-D-thiogalactopyranoside when the culture reached an OD_{600} between 0.4 and 0.6. After 8 h at 37 °C the cells were harvested by centrifugation and suspended in 10 mL of lysis buffer (100 mM Tris, pH 7.9, 300 mM NaCl, and 10 mM imidazole) per gram of cells. The suspension was made to 0.1% PMSF and 1 mg/mL lysozyme, stored on ice for 30 min, and disrupted by passing twice through the French press. The lysate was centrifuged to remove the cellular debris. The supernatant was taken to 20% saturation with ammonium sulfate and centrifuged, and the supernatant was applied to a 10 mL Ni-NTA resin column previously equilibrated with

wash buffer (20 mM imidazole, 100 mM Tris, pH 7.9, and 300 mM NaCl). The column was washed with 5 volumes wash buffer, and the His_6 N-terminal tagged MTAP was eluted with 10 volumes of the elution gradient (30−300 mM imidazole, 100 mM Tris, pH 7.9, and 300 mM NaCl). The MTAP peak was concentrated to 8 mg/mL and dialyzed against 100 mM Tris, pH 7.9, 50 mM NaCl, and 2 mM DTT. The purified protein was frozen rapidly (dry ice and ethanol) in small glass tubes and stored at −80 °C. The yield of enzyme is typically 8−10 mg/L of culture. The concentration of protein was determined by both Bradford and A_{280}. Its purity was determined to be >95% on the basis of SDS−PAGE using a 4−15% polyacrylamide gradient.

Enzymatic Assays and Inhibition. The spectrophotometric assay measured the conversion of MTA into adenine as a decrease in absorbance at 275 nm to give $\Delta\epsilon$ between MTA and adenine of 1.6 mM^{-1} cm^{-1}. Inhibitor concentrations were determined by the ultraviolet absorbance spectrum using the extinction coefficients for 9-deazadenine of 8.5 mM^{-1} cm^{-1} at 275 nm at pH 7.0. The kinetics for slow-onset inhibition and the K_i measurement were carried out by adding enzyme of known concentration (1−5 nM) to the reaction mixtures at 25 °C containing up to 2 mM MTA and 100 mM potassium phosphate, pH 7.4. At high concentrations of MTA, 0.1 cm path length spectrophotometer cells were used. The substrate concentration of 200 μM MTA, and 100 mM phosphate was used for routine MTAP assays. The K_{eq} for the MTAP reaction (MTA + PO_4 ↔ adenine + 5-methylthio-α-D-ribose 1-PO_4) is approximately 10^{-3} under these conditions; therefore, the initial rate period is shortened by the approach to equilibrium, even at 100 mM phosphate. In cases where irreversible reactions are desirable, the reaction was conducted in 100 mM Hepes buffer, pH 7.4, containing 50 mM sodium arsenate as the nucleophile and 0.1 mM DTT. This makes the reaction chemically irreversible since ribosyl 1-arsenates are unstable and hydrolyze rapidly. Conditions for K_i* determination used high concentrations of substrate relative to the reported K_m of 5 μM for native and cloned MTAP (*13*). Controls having no inhibitor and no enzyme were included in all experiments. The K_i values for the inhibitors were calculated by fitting the initial rates to the expression for competitive inhibition:

$$\frac{V_0'}{V_0} = \frac{K_m + [S]}{K_m + [S] + K_m[I]/K_i}$$

where V_0' is the rate in the presence of inhibitor, V_0 is the rate in the absence of inhibitor, [I] is the inhibitor concentration, and [S] is the substrate concentration. These relationships are valid only when the concentration of the inhibitor is at least 10-fold greater than enzyme concentration (*14*).

Tight-binding transition state analogue inhibitors often display a second phase of tighter inhibition after reaching a thermodynamic equilibrium with the enzyme. This dissociation constant is the K_i* value and is calculated by fitting to the expression for competitive inhibition:

$$\frac{V_s'}{V_s} = \frac{K_m + [S]}{K_m + [S] + K_m[I]/K_i*}$$

after the reaction has reached its equilibrium value of slow-onset inhibition. These equations assume competitive inhibition, and the X-ray crystal structures ensure that the substrate and inhibitors bind at the same site.

Table 1: Data Collection and Refinement Statistics

Data Collection	
space group	*P*321
unit cell	
a (Å)	122.231
c (Å)	44.743
resolution limits (Å)	20−1.95 (2.02−1.95)[a]
completeness (%)	99.5 (100.0)
R_{sym} (%)	6.4 (38.6)
no. of reflections	
unique	28021
total	167189
Structure Refinement	
R_{cryst} (%)	18.0
R_{free} (%)	20.7
no. of amino acids	273
no. of waters	132
no. of ligands	1 MT-ImmA, 1 phosphate
av protein *B*-factor (Å^2)	18.9
av ligand *B*-factor (Å^2)	13.6
av water *B*-factor (Å^2)	25.5
RMS deviations	
bond (Å)	0.005
angle (deg)	1.3

[a] Values in parentheses are for the highest resolution shell.

Inhibitor Synthesis. MT-immucillin-A and phenylthio-immucillin-A were synthesized via desilylation of *N-tert*-butoxycarbonyl-7-*O-tert*-butyldimethylsilyl-2,3,6-trideoxy-3,6-imino-4,5-*O*-isopropylidene-D-*allo*-heptononitrile (*15*), methanesulfonylation of the deprotected C-7 hydroxyl group, and displacement of the sulfonate with either sodium thiomethoxide or sodium thiophenoxide to afford *N-tert*-butoxycarbonyl-7-methylthio-2,3,6-trideoxy-3,6-imino-4,5-*O*-isopropylidene-D-*allo*-heptononitrile or N-*tert*-butoxycarbonyl-7-phenylthio-2,3,6-trideoxy-3,6-imino-4,5-*O*-isopropylidene-D-*allo*-heptononitrile, respectively. Previously reported methods were then used to construct the 9-deazaadenine subunits and globally deprotect (*15*) to afford the bishydrochloride salts of MT-immucillin-A and phenylthio-immucillin-A.[2]

MT-DADMe-immucillin-A, phenylthio-DADMe-immucillin-A, and *p*-Cl-phenylthio-DADMe-immucillin-A were synthesized via selective methanesulfonylation of the hydroxymethyl group of the previously reported (3*R*,4*R*)-*N-tert*-butoxycarbonyl-3-hydroxy-4-hydroxymethylpyrrolidine (*16*) followed by displacement of the sulfonate group with either sodium thiomethoxide, sodium thiophenoxide, or sodium 4-chlorophenylthiolate and deprotection of the Boc group with methanolic HCl to afford either (3*R*,4*S*)-3-hydroxy-4-(methylthiomethyl)pyrrolidine hydrochloride, (3*R*,4*S*)-3-hydroxy-4-(phenylthiomethyl)pyrrolidine hydrochloride, or (3*R*,4*S*)-3-hydroxy-4-(4-chlorophenylthiomethyl)pyrrolidine hydrochloride, respectively. Conversion of these amine hydrochlorides to the DADMe-immucillin-A derivatives was achieved via a Mannich reaction with formaldehyde and 9-deazaadenine as previously described (*17*).[2]

[2] A detailed description of the synthesis and characterization of these and related compounds will be published elsewhere. The steps described here establish the synthetic strategy and document literature methods for the chemical steps.

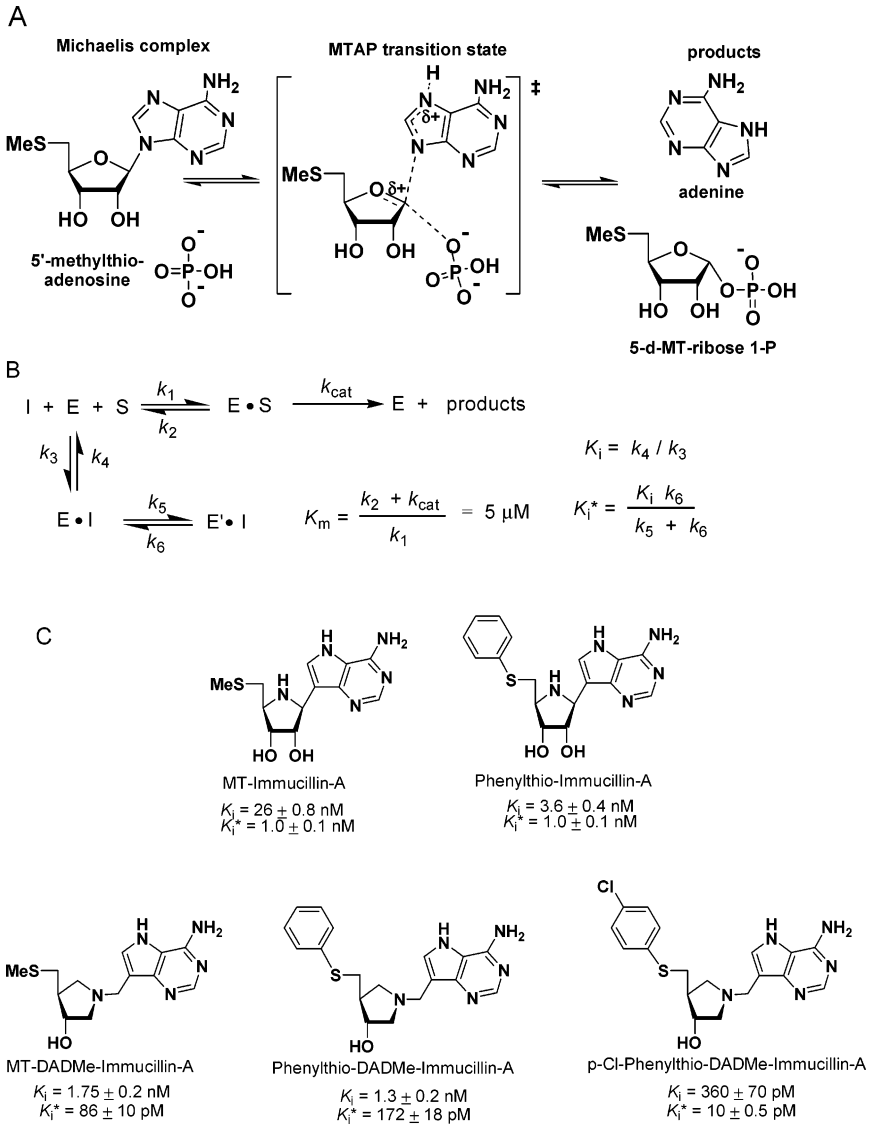

FIGURE 2: Reaction catalyzed by MTAP (A). Oxacarbenium transition states occur in all known *N*-ribosyltransferases. Steps in the slow-onset, tight binding of transition state analogue inhibitors (B) are shown, where I, E, S, and E′ are inhibitor, enzyme, substrate, and enzyme with tightly bound inhibitor following slow onset. K_i and K_i* are the dissociation constants for inhibitors taken with initial rate and equilibrium conditions, respectively. Immucillin inhibitors designed to be transition state analogues of MTAP (C).

Crystallization of MTAP·MT-ImmA·PO₄. Recombinant human MTAP was cocrystallized with a 1:2 stoichiometry of MT-ImmA and 5 mM phosphate by hanging-drop vapor diffusion at 18 °C. Protein (2.5 μL of 15 mg/mL) containing MT-ImmA and phosphate was mixed with 0.5 μL of 100 mM spermidine and 2.0 μL of a reservoir solution containing 100 mM Tris, pH 8.0, and 20% PEG 6000 (Hampton) and equilibrated against 1 mL of reservoir solution. Long rods with hexagonal faces appeared in 3 days and grew to 50 × 50 × 500 μm^3. Diffraction patterns from the crystals were consistent with the space group *P*321 ($a = b = 122.23$ Å, $c = 44.74$ Å), with a monomer in the asymmetric unit ($V_m = 3.09$ Å^3/Da; 60% solvent).

Data Collection, Processing, and Structure Determination. Crystals were transferred briefly to reservoir solution containing 5−25% glycerol and frozen at −178 °C. X-rays from beamline X9B (Brookhaven National Laboratory, 0.98 Å) were diffracted by the crystals, and data were collected on a 2 × 2 ADSC Quantum CCD detector. Data for the MTAP·MT-ImmA·PO_4 were reduced with the HKL programs (*18*) and were 99.5% complete to 1.95 Å resolution with R_{sym} of 6.4%. In the last shell (2.02−1.95 Å), 86% of the reflections had $I/(\sigma)I > 1.0\sigma$ with R_{sym} of 38.6%. Crystals were isomorphous with MTAP·MTA·SO_4 reported earlier by the Ealick laboratory (*19*). Rigid-body refinement gave an initial *R*-factor of 35.2% and a correlation coefficient of 66.7% using 8.0−4.0 Å data.

Structure Refinement. The structure of MTAP·MT-ImmA·PO_4 was refined with CNS (*20*) and manual intervention using the program O (*21*). The final model includes residues 9−281, MT-ImmA, a phosphate ion for each monomer, and 132 water molecules with R_{cyrst} and R_{free} of 18% and 20.7%, respectively. Contacts at subunit interfaces were identified by Contactsym (*22*). Analysis by PROCHECK (*23*) indicates excellent stereochemistry with 89.4%, 9.8%, and 0.4% in the most favored, additionally allowed, and generously allowed regions of the Ramachandran plot, respectively. Lys51 is in the disallowed region but shows excellent electron density in $F_o - F_c$ omit maps. The parameters for data collection and structure refinement are provided in Table 1. The structure has been deposited in the Protein Data Bank (PDB ID code 1K27).

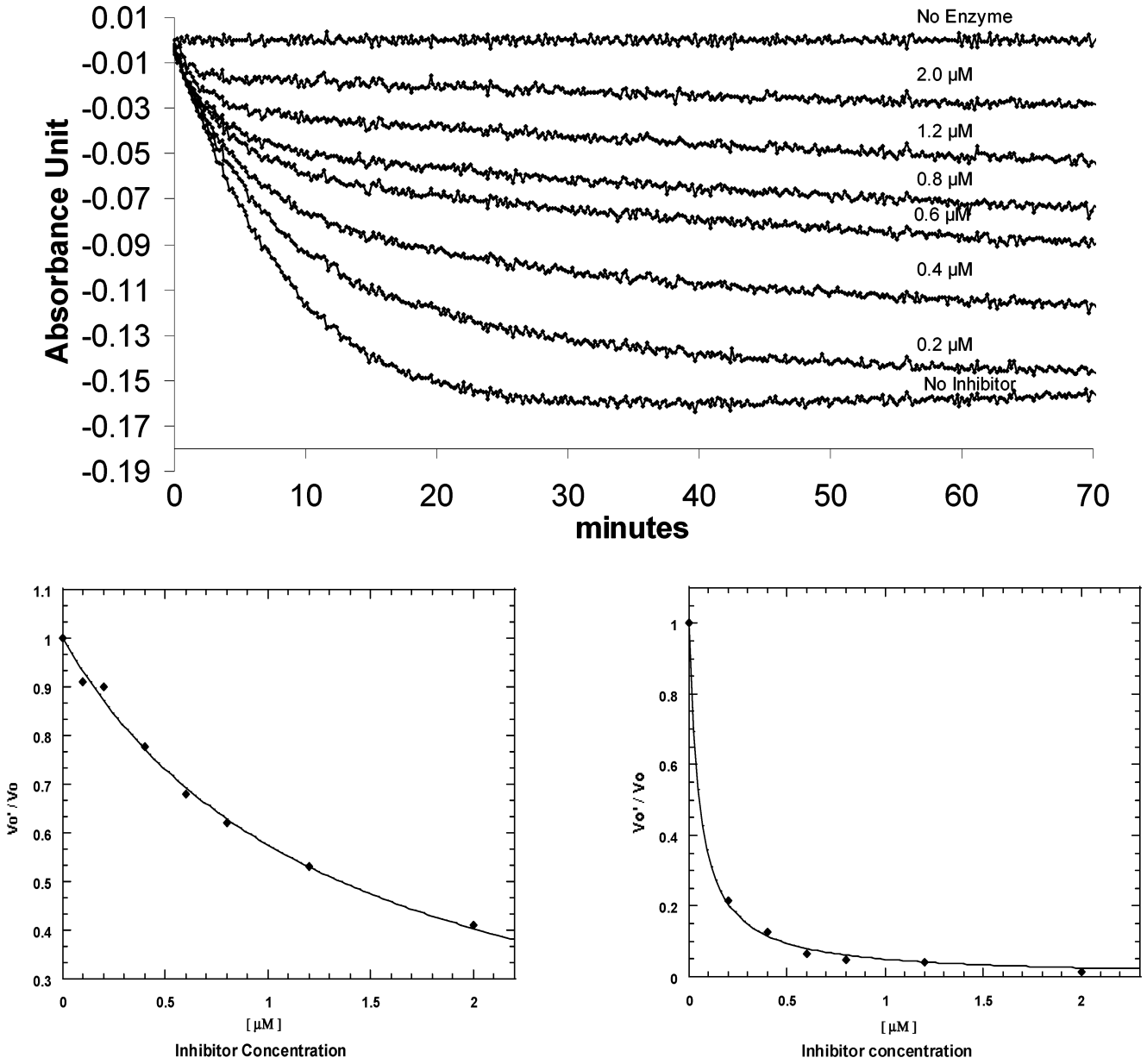

FIGURE 3: Slow-onset inhibition of MTAP by MT-ImmA (upper panel). MTA and phosphate were at 250 μM and 100 mM, respectively. Values of K_i (lower left) and K_i* (lower right) from fits of initial and final reaction rates. Similar experiments gave the values shown in Figure 2C.

RESULTS AND DISCUSSION

Inhibitors of MTAP. The phosphorolysis chemistry catalyzed by MTAP is closely related to that of PNP, and the protein fold and catalytic site arrangement are similar despite the modest 24.5% amino acid sequence identity (Figure 2A; *19*). The immucillins and DADMe-immucillins are powerful transition state analogues of human PNP by mimicking the ribooxacarbenium ion of the transition state when bound to the enzyme (*7*−*9*). MT-immucillin-A was synthesized as a transition state analogue of MTAP on the hypothesis that the transition state structure resembles that of PNP. MT-ImmA is an oxacarbenium ion mimic of a dissociative transition state (Figure 2A,C). All known transition states for *N*-ribosyltransferases have oxacarbenium characteristics but lack the oxacarbenium-stabilizing catalytic site carboxylates found in glucosyltransferases (*24*). MT-ImmA is a slow-onset tight-binding inhibitor with a K_i value of 26 nM and a K_i* equilibrium dissociation constant of 1 nM (Figure 3). The K_m value was determined for our overexpression construct of human MTAP and was 5 μM for MTA, to give a K_m/K_i* ratio of 5000. The crystal structure of MTAP indicated a flexible hydrophobic pocket near the 5′-thiomethyl group (see below), and replacement of the 5′-methyl group with a phenyl group in phenylthio-immucillin-A gave K_i and K_i* values of 3.6 nM and 1.0 nM, respectively (Figure 2C). On the basis of the recent finding that the related DADMe-immucillin-H family exhibits tight binding to human PNP (*9*), MT-DADMe-immucillin-A was synthesized and gave K_i and K_i* values of 1.75 nM and 86 pM, respectively, for a K_m/K_i* ratio of 58000. In dissociated *N*-ribosyl transfer transition states the distance between C1′ of the ribosyl group and the N9 of the departing nucleophile is near 3 Å, and the use of a methylene bridge to separate the oxacarbenium center and the leaving group improves the

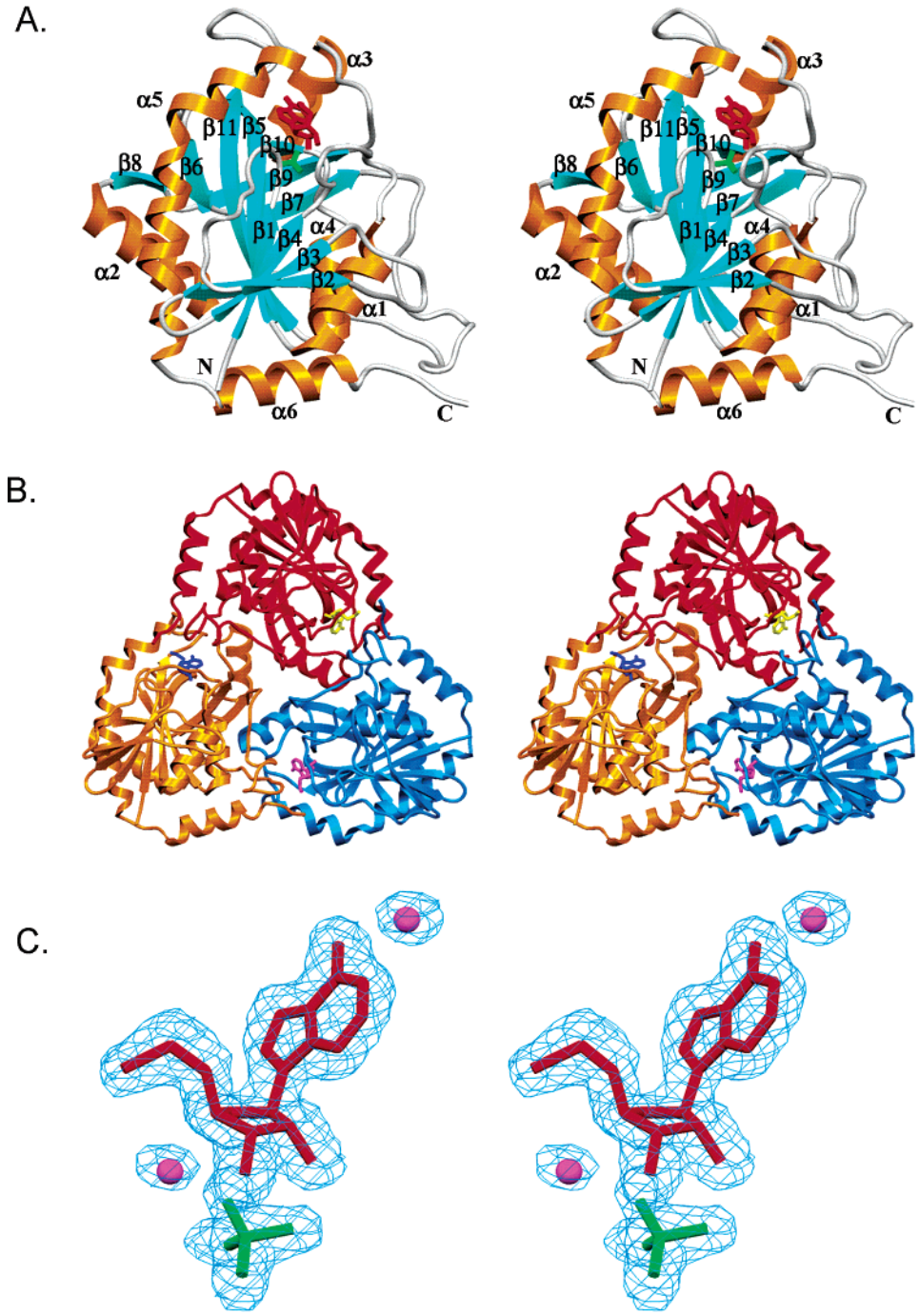

FIGURE 4: Stereo ribbon diagrams of human MTAP monomer with bound MT-ImmA (A) and the trimer (B). Stereoview of the $F_o - F_c$ electron density omit map contoured at 2.5σ for bound MT-ImmA, phosphate, and two ordered water molecules (C). The active sites are located near the trimer interface. This figure and Figure 5 were generated using SETOR (*27*).

similarity to the transition state (*9*). Combining the 5′-phenylthio group and the methylene bridge in the DADMe compound gives phenylthio-DADMe-immucillin-A (Figure 2C). This compound gave K_i and K_i* values of 1.3 nM and 172 pM for a K_m/K_i* ratio of 29000. Not all of the residues near the 5′-thiomethyl group of MT-ImmA are hydrophobic. For example, His137B is contributed from the neighboring subunit by a flexible loop that closes over the catalytic site of the neighboring subunit. An attempt was made to engage both the hydrophobic pocket with a phenyl group and an electrostatic interaction with H-bond donor groups (e.g., His137B or peptide amides). *p*-Cl-phenylthio-DADMe-immucillin-A gave K_i and K_i* values of 360 and 10 pM for a K_m/K_i* ratio of 500000. This inhibitor is the tightest binding inhibitor reported for MTAP with affinity similar to the best PNP inhibitors (*9*).

Structure of MTAP·MT-ImmA·PO4. Human MTAP is a symmetric homotrimer similar to human PNP with a single domain of 11 β strands and 6 α helices (Figure 4; *19*, *25*). The core has a mixed 8-stranded β sheet (residues are β2, 29−33; β3, 45−50; β4, 54−59; β1, 11−16; β5, 87−98; β11, 210−220; β6, 106−110; and β8, 161−164) with β5 and β11 extended to create a 5-stranded β sheet (β11; β5; β10, 192−195; β9, 160−172; β7, 112−116) surrounded by 6 α helices (α1, 73−84; α2, 146−159; α3, 180−189; α4, 200−208; α5, 233−259; α6, 264−274). MTAP crystals have a

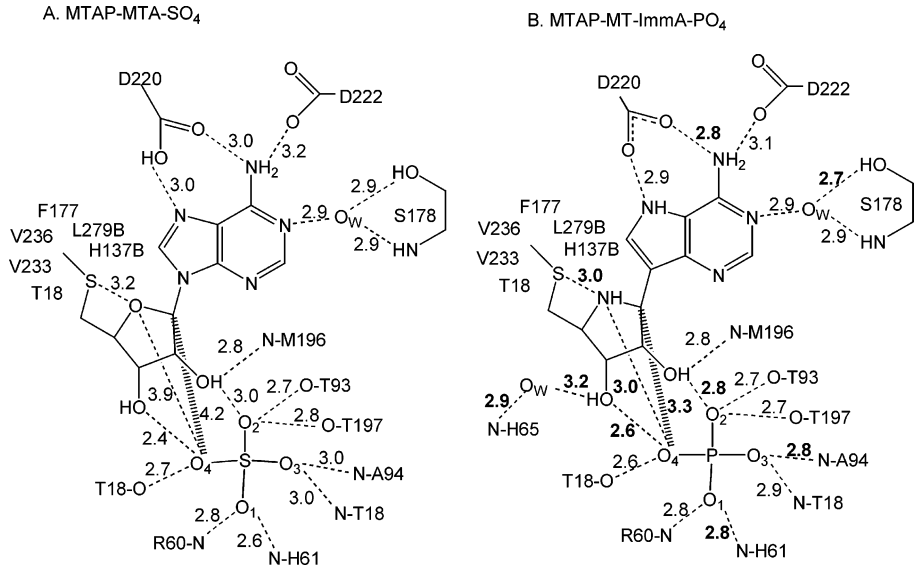

FIGURE 5: Catalytic site contacts for (A) MTAP·MTA·SO_4 (*19*) and (B) MTAP·MT-ImmA·PO_4 complexes. Side chains displayed here are involved in hydrogen bond or van der Waals contacts with the components at the catalytic sites. The catalytic site residues in MTAP are amino acid contacts from a single subunit, except for His137B and Leu279B from loops in the neighboring (B) monomer. Distances are in angstroms, and significant changes in the MT-ImmA structure are in bold.

monomer in the asymmetric unit, and the MTAP trimer axis is coincident with the crystallographic 3-fold symmetry axis (Figure 4). Subunit interfaces are extensive, burying 2500 Å^2 from each monomer. The interface involves a loop connecting β4 to α1 (64−71), β7 (116−119), α3 (175−189), and α5 (233−237) from one monomer interacting with β7 and the loop connecting β7 to α2 (112−141) and the C-terminal residues 276−281 from the neighboring monomer. Two salt bridges, 12 hydrogen bonds, and 145 van der Waals interactions (4.0 Å or less) stabilize the interface. The His_6 tag at the N-terminus was disordered, is located far from the catalytic site, and did not alter the K_m value reported for the native enzyme (*13*).

Contacts to MT-ImmA and PO_4. The catalytic sites in MTAP are near the subunit interfaces with contacts dominated by the parent residue but where His137 and Leu279 from the neighboring subunit participate in hydrophobic interactions with the 5′-methylthio group. Analysis of the difference Fourier maps ($F_o - F_c$) and refined *B*-factors indicates that the catalytic sites are fully and equally occupied by MT-ImmA and PO_4 (Figure 4C). MT-ImmA is bound between the small β sheet (β11−β5−β10−β9−β7) and neighboring loops with phosphate bound at the bottom of the active site in close proximity to C1′ and N4′ of the iminoribitol ring (3.3 and 3.0 Å, respectively; Figures 5 and 6A). The 5′-methylthio group is located in a primarily hydrophobic pocket formed by Thr18, Val 233, Val236, and Phe177 from the parent monomer and His137B and Leu279B from the adjacent monomer. The 9-deazaadenine group is wedged between the backbone of the 5-stranded β sheet and the side chain of Phe177 (Figure 6A). Hydrogen bonds are formed between Asp220, the 6-amino group, and N7 (2.8 and 2.9 Å, respectively). The pK_a of N7 in the immucillins is >10, and Asp220 must be anionic to accept two favorable hydrogen bonds from NH7 and $NH_2$6 of MT-ImmA. In the Michaelis complex with MTAP, the N7 of MTA has a pK_a near 2,[3] and Asp220 must be neutral to donate a H-bond to N7 and to accept a H-bond from $NH_2$6 (*19*). Asp220 is ideally located to act as the general acid to donate/accept a proton at N7 while anchoring the reactant molecule by the 2.8 Å H-bond at the 6-amino group.

Oxacarbenium character is present at the transition states of all reported *N*-ribosyltransferases (*24*). The N4′-imino group of immucillin iminoribitols[4] has a pK_a of 6.9 and is known to be cationic at the catalytic sites of *N*-ribosyltransferases (*26*). Similar to other purine *N*-ribosyltransferases, there are no enzymatic carboxyl groups to interact with the N4′-oxacarbenium ion mimic, and the nearest protein atom to the N4′ is OG of Thr18 at 3.9 Å (not shown). The nearest neighbor to N4′ is O4 of bound phosphate at 3.0 Å, and this oxygen is 3.3 Å below C1′, the electrophilic center for the reaction. In the structure of human MTAP·MTA·SO_4, the nucleophilic oxygen to C1′ distance was 4.2 Å (*19*), and the closer 3.3 Å for MTAP·MT-ImmA·PO_4 reflects the formation of the ion pair that mimics the ion pair that forms in the transition state.[5] The *N*-ribosyltransferases operate through a mechanism called "nucleophilic displacement by electrophile migration" in which relatively fixed phosphate and purine nucleophiles are activated by enzyme-enforced interactions and the ribooxacarbenium ion migrates between the fixed nucleophiles in the reaction coordinate. The interactions with MT-ImmA and phosphate at the catalytic site of MTAP are consistent with this mechanism. On the basis of the geometry and distances of bound MT-ImmA, a 1.8 Å migration of C1′ toward the fixed phosphate anion would constitute the reaction coordinate. This distance for

[3] The pK_a for protonation of N1 of adenosine (and therefore MTA) in solution is approximately 4.0, making the pK_a at N7 significantly less than 4. After protonation of N1, N7 protonation forms the dication near pH 1. In MTAP the enzyme forms a water H-bond to N1 of MTA, and this would influence the pK_a at N7. We can estimate that N7 of MTA in the Michaelis complex with MTAP has a pK_a of 2 ± 1.

[4] Immucillin-H is (1*S*)-1-(9-deazahypoxanthin-9-yl)-1,4-dideoxy-1,4-imino-D-ribitol and has been shown to have a pK_a >10 at N7 (*26*). MT-ImmA is chemically similar in the 9-deazaadenine ring and is expected to have a similar pK_a.

[5] Kinetic isotope effect studies with human MTAP establish the oxacarbenium nature of the transition state (Singh and Schramm, unpublished results).

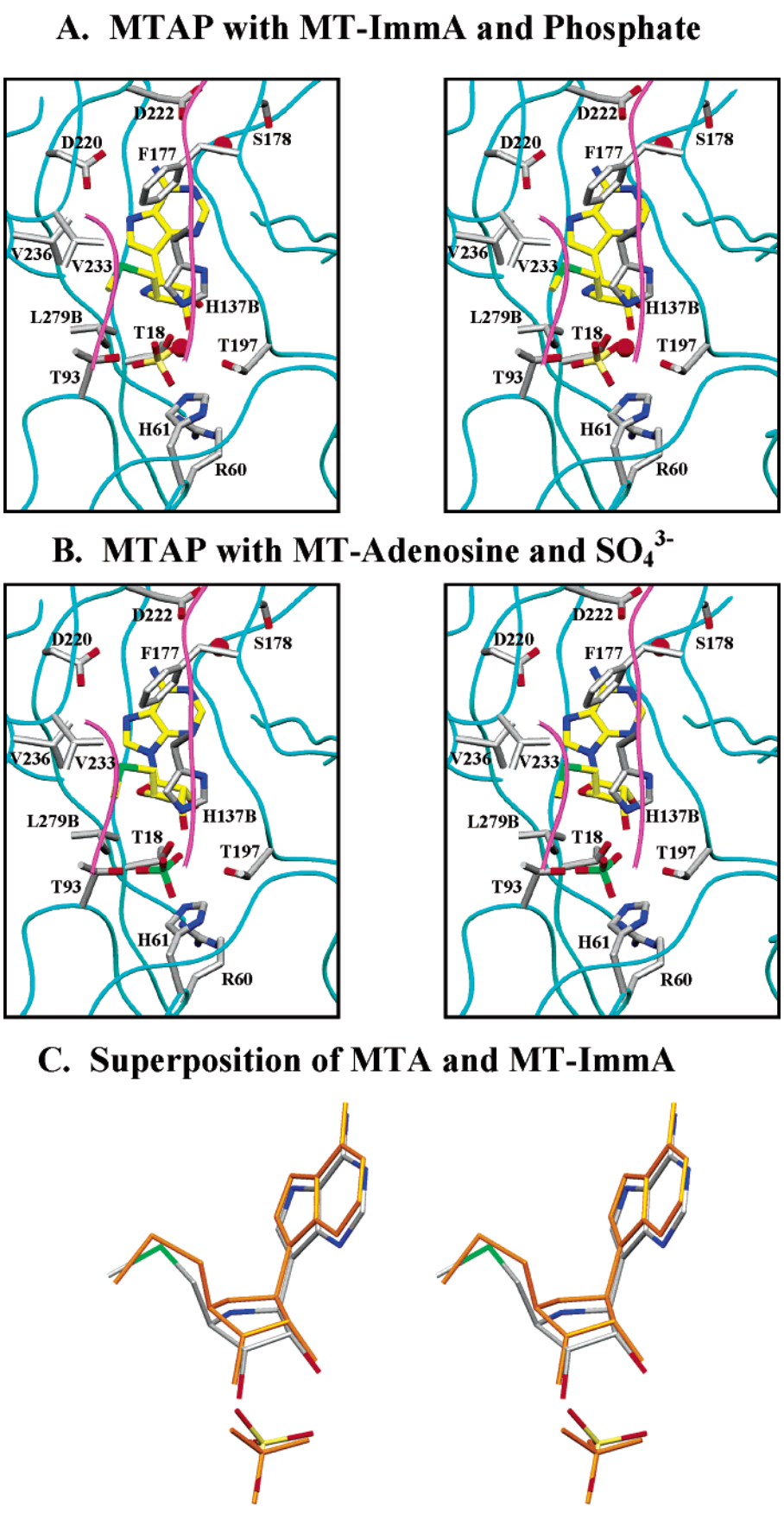

FIGURE 6: Stereoview of the amino acids in the active site of human MTAP·MT-ImmA·PO_4 (A) and human MTAP·MTA·SO_4 (B). The superposition (C) shows the relative alignment and geometry of MTA (gold) and MT-ImmA (C, gray; N, blue; O, red; P, yellow; S, green) at the catalytic sites of these complexes. Both ligands were aligned with backbone segments of the protein that are constant in both complexes.

electrophilic migration is similar to that found at the catalytic site of bovine PNP (*25*). Other contacts to the iminoribitol include a water-mediated H-bond between His65 and O3′ and a direct 2.8 Å H-bond between Met196 and O2′.

Together with the phosphate interaction, these contacts orient the iminoribitol relative to the phosphate.

Activation of the phosphate anion is through Arg60 and His61 to O1 and a bidentate interaction of Thr18 contacts O3 and O4. Hydrogen bonds between O2, Thr93, and Thr197 complete the seven direct H-bonds (of less than 3.0 Å) to phosphate, all provided by loops in the protein structure (Figures 5 and 6). These contacts leave O4 positioned for access by the migration of the ribosyl C1′.

Structural Comparison of MTAP·MTA·SO_4 and MTAP·MT-ImmA·PO_4. MTAP transition state analogue and substrate complexes are similar with an RMS deviation of 0.3 Å for all Cα atoms. The 5′-methylthio group and the adenine/9-deazaadenine bases participate in similar hydrogen-bonding networks in the two structures (*19*). Despite this similarity, N7 is a H-bond acceptor with MTA and a donor with MT-ImmA. Thus Asp220 must be a neutral H-bond donor in the Michaelis complex or, if ionized in this complex, will form a repulsive interaction with N7. In contrast, the carboxyl of Asp220 forms an anionic H-bond acceptor with N7 of MT-ImmA. A water-mediated hydrogen bond between His65 and O3′ is observed in MTAP·MT-ImmA·PO_4 but not in the MTAP·MTA·SO_4 complex, despite the similar crystallization conditions and resolution ranges. Another difference between the complexes lies in the disposition of the two ligands in the catalytic sites. In the MTAP·MT-ImmA·PO_4 complex, the phosphate O4 is at distances of 3.0 and 3.3 Å from the transition state analogue N4′ and C1′, respectively. In the MTAP·MTA·SO_4 complex, O4 of sulfate is 3.9 and 4.2 Å from the substrate MTA O4′ and C1′, respectively. These differences are caused by the more favorable binding interactions of the transition state analogue inhibitor to organize the protein around the catalytic site and to pull the transition state analogue slightly deeper into the catalytic site (Figure 6C).

Purine nucleosides prefer the C3′-*endo* conformation (C3′ above the plane of the ribose ring) in solution. The ribooxacarbenium ion transition states of *N*-ribosyltransferases are characterized by ribosyl rings in which C1′ approaches sp^2 hybridization, and the ribosyl ring pucker is C3′-*exo* (C3′ below the plane). In both MTAP·MT-ImmA·PO_4 and MTAP·MTA·SO_4 complexes the iminoribitol and ribosyl groups have C3′-*exo* pucker imposed by the enzyme in preparation for transition state formation.

Basis for Tight Binding of Immucillins. The hydrogen bond lengths to MTA·SO_4 and MT-ImmA·PO_4 are similar and would not predict large differences in binding energy from the ensemble of H-bond distances alone. However, two transition state features of MT-ImmA readily account for the observed pM binding constant. MTA is a neutral molecule, and the interaction between O4 of phosphate and O4′ of the ribosyl ring is a repulsive one since both are electron rich and carry partial negative charges. The distance of 3.9 Å reflects this electronic repulsion (Figure 5). In contrast, the same atomic position in MT-ImmA is the 4′-imino cation that forms a 3.0 Å ion pair to the O4′ of phosphate. Although we cannot solve Coulomb's law explicitly for this case since the dielectric constants are unknown and differ between the charged and uncharged molecules, a conservative estimate is to separate the phosphate anion from the MT-ImmA imino cation from 3.0 to 3.9 Å assuming a dielectric of 5. This approximation gives over 10 kcal/mol binding energy, more than required to explain the 500000-fold increase in binding equilibrium.

A second interaction is that between Asp220 and N7 of bound MTA and MT-ImmA. On the basis of the crystal structure Asp220 provides a 3.0 Å hydrogen bond to N7 of MTA, requiring Asp220 to be protonated and to form a H-bond partner with N7, a group with pK_a near 2. MT-ImmA is protonated at N7 (pK_a > 10)[4] and donates a proton to anionic Asp220. Although the oxygen−nitrogen distance does not change, the H-bond to N7 of MT-ImmA is likely to be more favorable.

Several interactions with the phosphate anion are more favorable in the complex with MT-ImmA (bold in Figure 5B), consistent with an ion pair between the MT-ImmA and phosphate, pulling both more tightly into the catalytic pocket to more closely resemble the transition state complex.

Binding of DADMe-Immucillins. Although crystallographic information is not yet available for MTAP in complex with a DADMe-immucillin, structures have been solved for trimeric PNP with immucillin-H and DADMe-immucillin-H bound at the catalytic sites (*28*). In these cases the phosphate−iminoribitol ion pair is separated by 3.1 Å in the complex with immucillin-H but only by 2.7 Å in the presence of DADMe-immucillin-H. In MTAP, shifting the nitrogen from the 4′ to 1′ position in the DADMe-immucillins increases affinity by 6−12-fold, and this reflects increased ion pair interaction and the loss of the 2′-hydroxyl interactions in the oxacarbenium mimic. Thus, the DADMe-immucillin-A analogues are proposed to form a more favorable ionic bridge to phosphate to enhance binding.

Conclusions. Transition state analogue mimics were designed on the proposal that MTAP is similar to other *N*-ribosyltransferases in having ribooxacarbenium ion character at its transition state. With dissociation constants to 10 pM, they are the most powerful noncovalent inhibitors reported for the polyamine pathway. They bind up to 500000 times tighter than substrate. The crystal structure with MT-immucillin-A indicates that the two features most similar to the transition state, namely, the 4′-iminoribitol cation and the elevated pK_a at N7 of the deazaadenine ring, play important roles in the tight binding. The tightest binding analogue is *p*-Cl-phenylthio-DADMe-immucillin-A and is proposed to capture binding energy from hydrophobic and electrostatic interactions at the hydrophobic 5′-binding pocket as well as from enhanced ion pair interactions between the 1′-nitrogen cation and nucleophilic phosphate anion.

REFERENCES

1. Tabor, C. W., and Tabor, H. (1976) *Annu. Rev. Biochem. 45*, 285−306.
2. Seiler, N., Atanassov, C. L., and Raul, F. (1998) *Int. J. Oncol. 13*, 993−1006.
3. Wallace, H. M., Fraser, A. V., and Hughes, A. (2003) *Biochem. J. 376*, 1−14.
4. McWilliams, M. L., Chen, G. D., and Fechter, L. D. (2000) *Toxicol. Sci. 56*, 124−132.
5. Thomas, T., and Thomas, T. J. (2003) *J. Cell. Mol. Med. 7*, 113−126.
6. O'Shaughnessy, J. A., Demers, L. M., Jones, S. E., Arseueau, J., Khandelwal, P., George, T., Gersh, R., Mauger, D., and Manni, A. (1999) *Clin. Cancer Res. 5*, 3438−3444.
7. Miles, R. W., Tyler, P. C., Furneaux, R. H., Bagdassarian, C. K., and Schramm, V. L. (1998) *Biochemistry 37*, 8615−8621.

8. Schramm, V. L. (2002) *Biochim. Biophys. Acta 1587*, 107−117.
9. Lewandowicz, A., Tyler, P. C., Evans, G. B., Furneaux, R. H., and Schramm, V. L. (2003) *J. Biol. Chem. 278*, 31465−31468.
10. Subhi, A. L., Diegelman, P., Porter, C. W., Tang, B., Lu, Z. J., Markham, G. D., and Kruger, W. D. (2003) *J. Biol. Chem.* (in press).
11. Ansorena, E., Garcia-Trevijano, E. R., Martinez-Chantar, M. L., Huang, Z. Z., Chen, L., Mato, J. M., Iraburu, M., Lu, S. C., and Avila, M. A. (2002) *Hepatology 35*, 274−280.
12. Harasawa, H., Yamada, Y., Kudoh, M., Sugahara, K., Soda, H., Hirakata, Y., Sasaki, H., Ikeda, S., Matsuo, T., Tomonaga, M., Nobori, T., and Kamihira, S. (2002) *Leukemia 16*, 1799−1807.
13. Ragione, F. D., Takabayashi, K., Mastropietro, S., Mercurio, C., Oliva, A., Russo, G. L., Pietra, V. D., Borriello, A., Nobori, T., Carson, D. A., and Zappia, V. (1996) *Biochem. Biophys. Res. Commun. 223*, 514−519.
14. Morrison, J. F., and Walsh, C. T. (1988) *Adv. Enzymol. Relat. Areas Mol. Biol. 61*, 201−301.
15. Evans, G. B., Furneaux, R. H., Gainsford, G. J., Schramm, V. L., and Tyler, P. C. (2000) *Tetrahedron 56*, 3053−3062.
16. Evans, G. B., Furneaux, R. H., Lewandowicz, A., Schramm, V. L., and Tyler, P. C. (2003) *J. Med. Chem. 46*, 5271−5276.
17. Evans, G. B., Furneaux, R. H., Schramm, V. L., and Tyler, P. C. (2003) *Org. Lett. 5*, 3639−3640.
18. Otwinowski, Z., and Minor, W. (1997) *Methods Enzymol. 276*, 307−326.
19. Appleby, T. C., Erion, M. D., and Ealick, S. E. (1999) *Structure 7*, 629−641.
20. Brunger, A. T., Adams, P. D., Clore, G. M.; DeLano, W. L., Gros, P., Grosse-Kunstleve, R. W., Jiang, J. S., Kuszewski, J., Nilges, M., Pannu, N. S., Read, R. J., Rice, L. M., Simonson, T., and Warren, G. L. (1998) *Acta Crystallogr. D54*, 905−921.
21. Jones T. A. (1985) *Methods Enzymol. B115*, 157−171.
22. Sheriff, S., Hendrickson, W. A., and Smith, J. L. (1987) *J. Mol. Biol. 197*, 273−296.
23. Laskowski, R. A., MacArthur, M. W., and Thorton, J. M. (1993) *J. Appl. Crystallogr. 26*, 283−291.
24. Schramm, V. L. (2003) *Acc. Chem. Res. 36*, 588−596.
25. Fedorov, A., Shi, W., Kicska, G., Fedorov, E., Tyler, P. C., Furneaux, R. H., Hanson, J. C., Gainsford, G. J., Larese, J. Z., Schramm, V. L., and Almo, S. C. (2001) *Biochemistry 40*, 853−860.
26. Sauve, A. A., Cahill, S. M., Zech, S. G., Basso, L. A., Lewandowicz, A., Santos, D. S., Grubmeyer, C., Evans, G. B., Furneaux, R. H., Tyler, P. C., McDermott, A., Girvin, M. E., and Schramm, V. L. (2003) *Biochemistry 42*, 5694−5705.
27. Evan, S. V. (1993) *J. Mol. Graphics 11*, 134−138.
28. Lewandowicz, A., Shi, W., Evans, G. B., Tyler, P. C., Furneaux, R. H., Basso, L. A., Santos, D. S., Almo, S. C., and Schramm, V. L. (2003) *Biochemistry 42*, 6057−6066.

BI0358420